Expanded View Figures

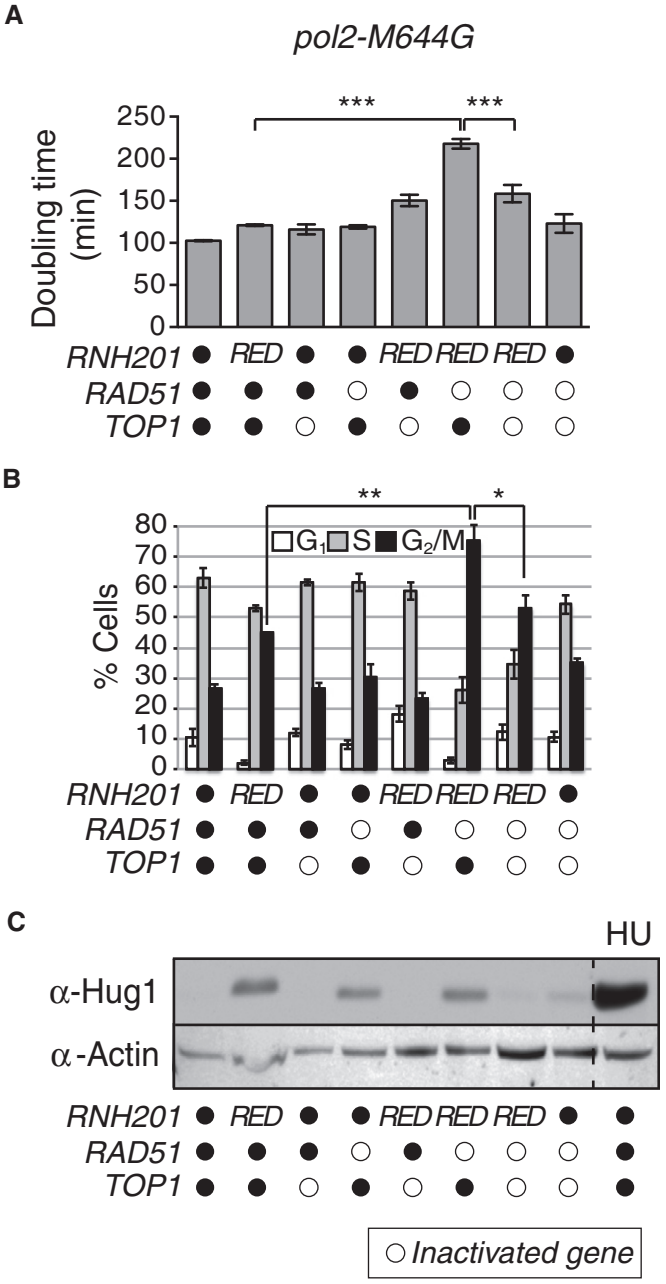

Figure EV1. Deletion of *RAD51* in a *rnh201-RED* strain causes genome instability phenotypes that are Top1 dependent.

All strains harbor the *pol2-M644G* mutation. Open circles indicate inactivated genes for each strain, and *RED* indicates *rnh201-RED* strain.

A Slow growth caused by loss of *RAD51* in a *pol2-M644G rnh201-RED* strain is Top1 dependent. Upper panel: Doubling times (D_t) were calculated for strains in the logarithmic phase of growth in rich medium at 30°C. ***$P \leq 0.001$ (unpaired Student's *t*-test in GraphPad Prism). The experiment was performed in triplicate. Data are displayed as the mean $D_t \pm$ standard deviation (SD).

B Flow cytometry analysis of cell cycle progression reveals that deletion of *RAD51* in a *pol2-M644G rnh201Δ* strain causes accumulation of cells in G_2/M phase in a Top1-dependent manner. Bar graphs display the percentage of cells in G_1, S, or G_2/M phase. The experiment was performed twice, and mean values ± SD are plotted. **$P \leq 0.01$ and *$P \leq 0.05$ (unpaired Student's *t*-test in GraphPad Prism).

C Activation of the genome integrity checkpoint was measured by immunoblotting for Hug1 in whole cell extracts from the indicated strains. Increase in Hug1 expression levels serves as a sensitive indicator of genome integrity checkpoint activation. Hydroxyurea (HU)-treated (200 mM for 3 h) cells served as a positive control.

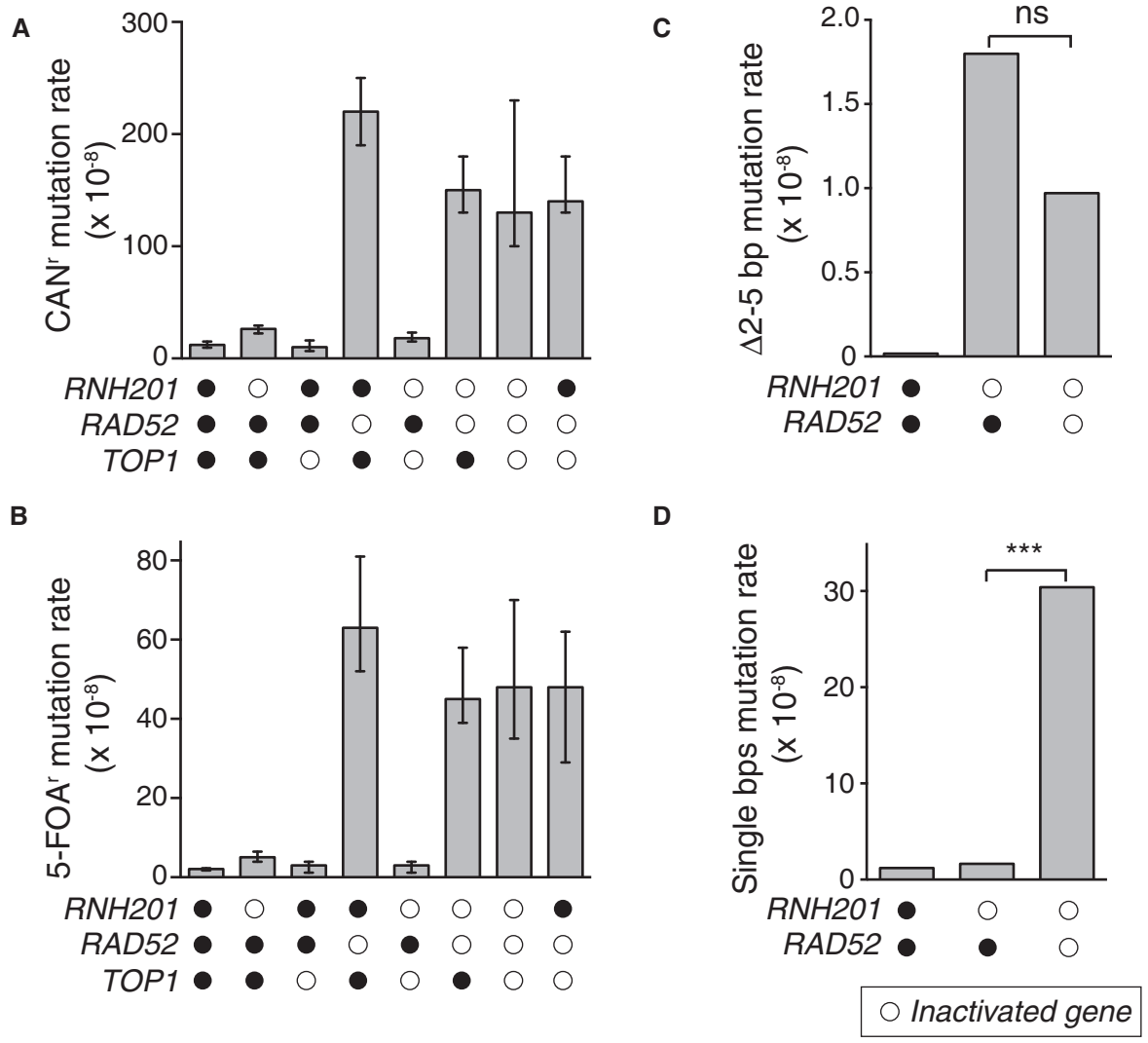

Figure EV2. Top1-dependent short deletions at unrepaired ribonucleotides occur independent of DSB repair.

Open circles indicate inactivated genes for each strain.

A, B (A) Overall *CAN1* mutation rates for strains with deletions of indicated genes. Spontaneous mutation rates were determined using fluctuation analysis as described previously (Shcherbakova & Kunkel, 1999). (B) Same as in panel (A), but for 5-FOA-resistance (5-FOA^r) conferred by mutation of the *URA3* reporter gene in orientation 2 adjacent to the *ARS306* replication origin (Nick McElhinny *et al*, 2008). Displayed are mean values ± the 95% confidence interval. The experiment was performed twice and mutation rate measurements were calculated for 24 independent isolates per genotype per experiment. Displayed are median values ± the 95% confidence interval.

C Displayed are 2–5 bp deletion mutation rates comparing *WT*, *rnh201*Δ, and *rnh201*Δ *rad52*Δ strains calculated from data listed in Appendix Table S1 for the *URA3-OR2* reporter. This rate was calculated using mutation spectra from Nick McElhinny *et al* (2010a) for the *WT* strain and from Clark *et al* (2011) for the *rnh201*Δ strain. 2–5 bp deletion rates were calculated by multiplying the proportion of this mutation type by the overall mutation rate for each strain. ns: $P = 0.089$ (Monte Carlo simulation) (Lujan *et al*, 2013). This demonstrates that the 2–5 bp deletion rate is not statistically significantly different when comparing the *rnh201*Δ strain to the *rnh201*Δ *rad5*Δ strain.

D Displayed are base pair substitution rates comparing *WT*, *rnh201*Δ, and *rnh201*Δ *rad52*Δ strains calculated from data listed in Appendix Table S1 for the *URA3-OR2* reporter. ***$P \leq 0.001$ (the rate is calculated as described in panel C).

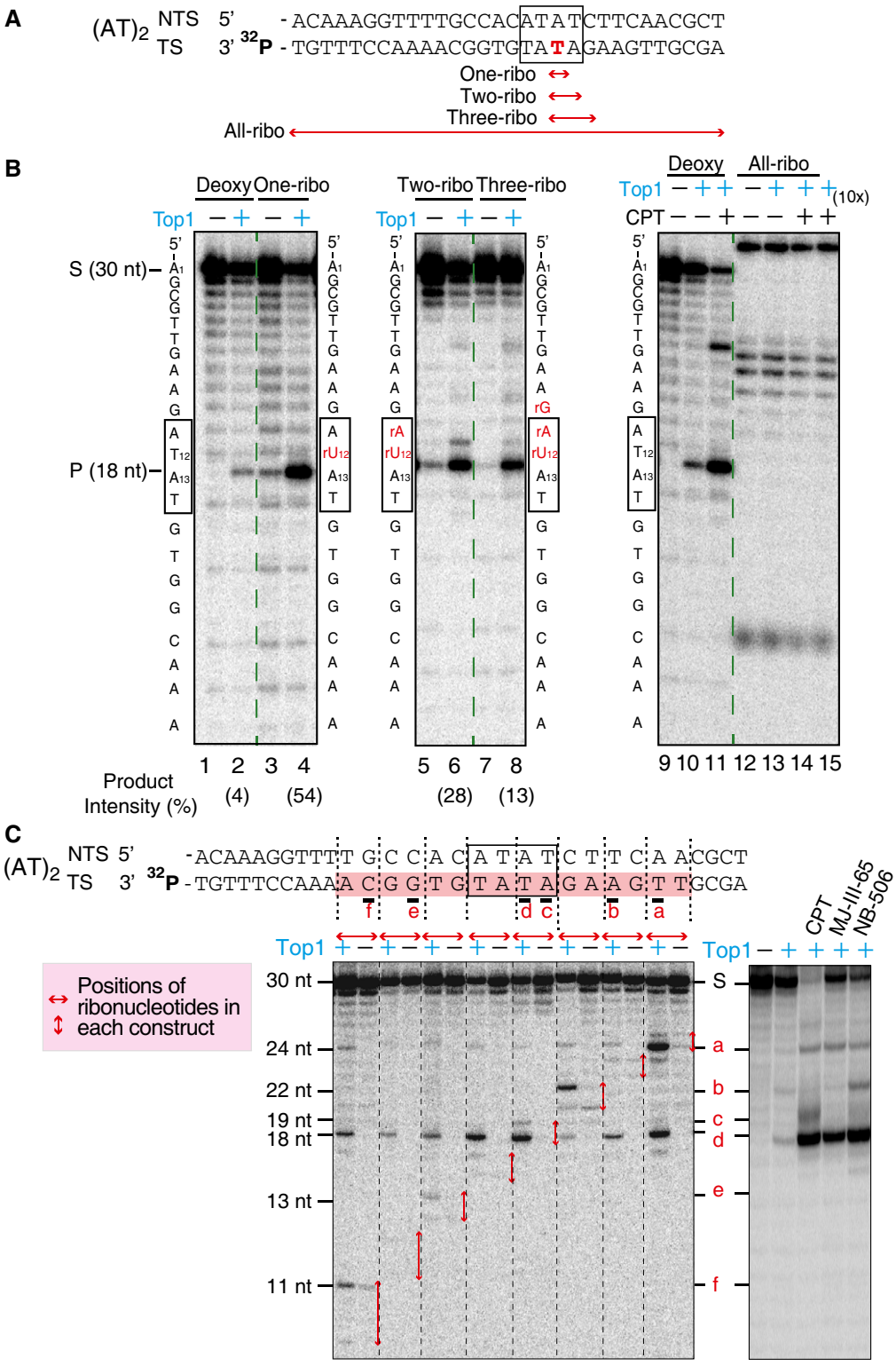

Figure EV3.

Figure EV3. Top1 ribonuclease activity cleaves at ribonucleotide sites at a high frequency, but increasing number of consecutive ribonucleotides diminishes Top1 cleavage sites gradually.

A DNA constructs contained sequences from the $(AT)_2$ site (marked by the black boxes) in the *CAN1* reporter gene, and the transcribed strand (TS) of each construct is radiolabeled on the 3′-end. Red double arrows indicate the positions of ribonucleotides in each construct. The constructs contain either zero, one, two, three, or all ribonucleotides at indicated positions.

B Top1 cleavage assay with DNA constructs with different number of ribonucleotides. The positions of the ribo-substitutions in each construct are indicated by red letters next to the gel panels. Product intensity is the amount of 18 nt Top1 cleavage products [P/(S + P)]. The results show that the presence of one ribonucleotide increased the Top1 cleavage product from 4% to 54%, while successive addition of ribonucleotides gradually decreases the percentage of Top1 cleavage product. All Top1 cleavage products are blocked with the All-ribo construct despite the presence of CPT and higher concentration of Top1 enzyme. The reactions contained 70 nM Top1 and 10 μM CPT where indicated, and the last sample with the All-ribo construct (lane 15) contained 700 nM Top1 recombinant protein (10×).

C To assess the frequency of Top1-induced DNA nicks at ribonucleotide sites, we carried out Top1 cleavage assays using DNA constructs with ribonucleotides incorporated at different positions. The constructs contained the $(AT)_2$ repeat sequence (marked by a box) from the *CAN1* reporter gene and were radiolabeled on the 3′-end of transcribed strand (TS). Each of the set of eight constructs contains two unique ribonucleotide substitutions (Appendix Table S3), and in total, a stretch of 16 nucleotides (shaded) on the TS sequence was examined. Lower left panel: representative gel image showing Top1 cleavage patterns for different constructs. Horizontal red double arrows mark the positions of ribonucleotide substitutions in each construct. The Top1-induced cleavage sites within ribonucleotide substitutions are labeled a–f next to the gel panels and below TS. The six Top1 sites identified include sites with Top1 covalent linkage to all four DNA bases, A, T, C, and G, deviating from the reported bias for a thymidine at the −1 position (covalently linked to Top1) (Jaxel *et al*, 1991; Parker & Champoux, 1993). Interestingly, the presence of ribonucleotides in some constructs, even at a distance, enhances Top1 cleavage (see site d), likely attributable to alteration in DNA local structures induced by ribonucleotides. Lower right panel: Top1 cleavage sites in the presence of three different Top1-trapping drugs with DNA construct containing only deoxyribonucleotides of the $(AT)_2$ sequence, radiolabeled on the 3′-end on the TS. The last three lanes contain additions of either CPT, indenoisoquinoline LMP774 (MJ-III-65) or indolocarbazole (NB-506). Only four out of six Top1 cleavage sites identified by ribonucleotide scanning were detected this way, labeled a–d next to the gel panels.

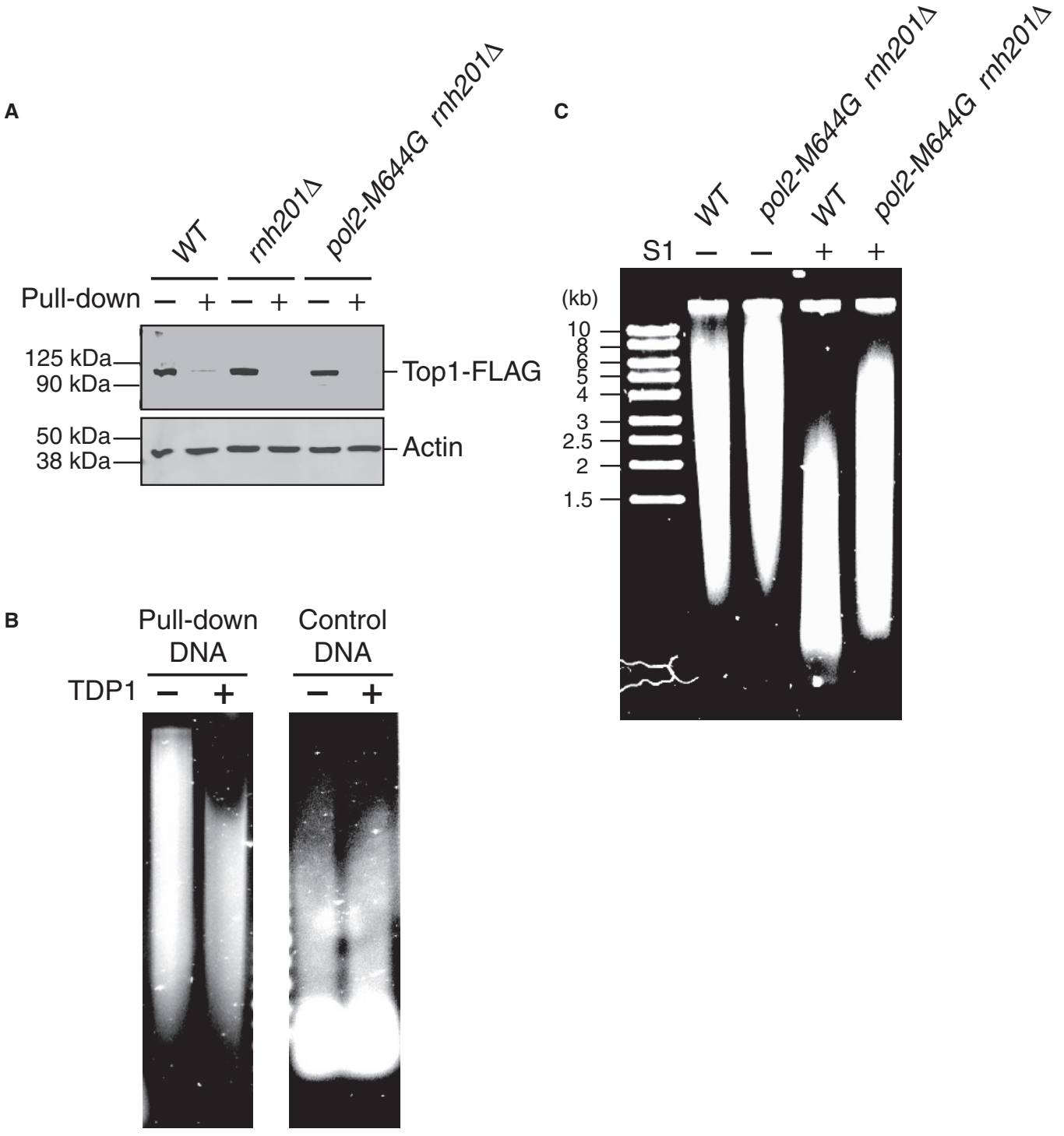

Figure EV4. Analysis of DNA covalently linked with Top1 by immuno-pull-down.

A Immunoblot of yeast cell lysates of different strains probing for the presence of 5×FLAG-tagged Top1 before (–) and after (+) immuno-pull-down with anti-FLAG antibodies.

B The DNA covalently linked with Top1 purified by immuno-pull-down (after proteinase K digestion) was further treated with 3 μM recombinant TDP1 overnight or mock-treated (Huang *et al*, 2013). TDP1-treated DNA showed increased gel mobility. The control DNA was purified from the same sample after the immuno-pull-down procedure and TDP1 treatment showed no effect on the control DNA.

C A representative gel image of mock-treated or S1-treated pulled-down DNA from either wild-type (*WT*) or *pol2-M644G rnh201Δ* strains.

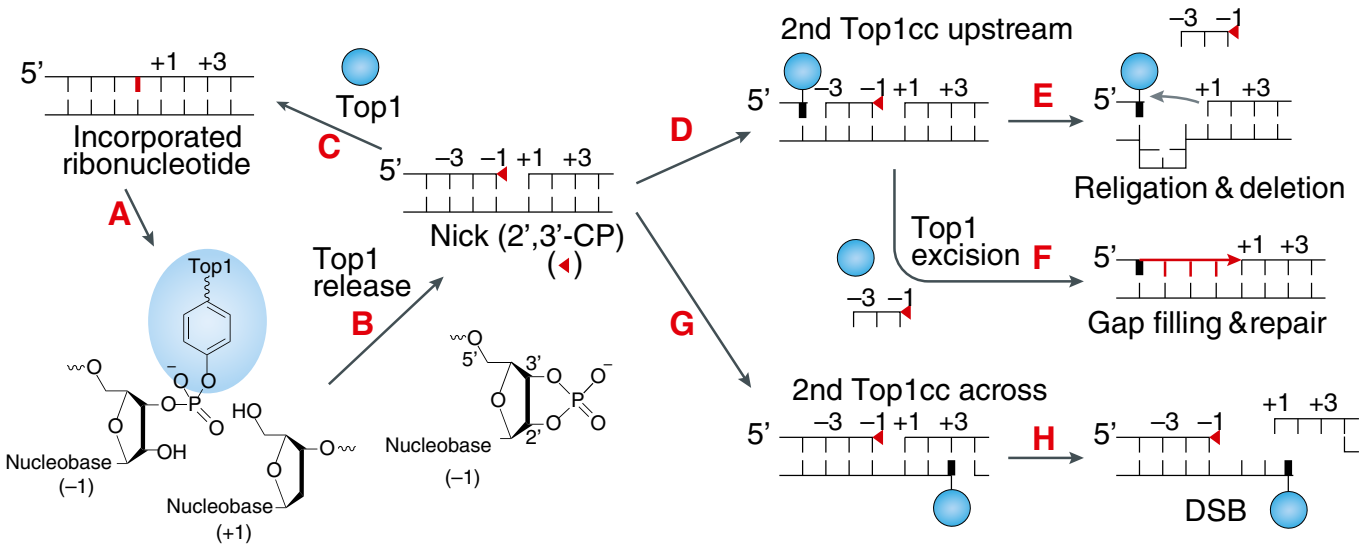

Figure EV5. Scheme of the different outcomes resulting from Top1 activity at incorporated ribonucleotides.

A Following ribonucleotide incorporation into the DNA (shown in red) during replication, a Top1cc forms at a ribonucleotide site.

B Top1cc is reversed by the nucleophilic attack of the 2′-ribose hydroxyl, which generates a 2′,3′-cyclic phosphate (2′,3′-CP) end (red triangle) and releases catalytically active Top1.

C Top1 can then bind to the nick, enabling nucleophilic attack of the 5′-ribose hydroxyl on 2′,3′-CP and facilitating religation of DNA backbone independently of its enzymatic activity (Huang *et al*, 2015).

D Sequential Top1 cleavage on the same strand, upstream of the 2′,3′-CP by the released Top1 or by another Top1 can lead to the loss of short DNA fragment containing 2′,3′-CP and persistent Top1cc.

E Realignment of DNA within the repeat sequence followed by religation can generate a short deletion (Kim *et al*, 2011; Cho *et al*, 2013; Huang *et al*, 2015).

F Alternatively, endonucleolytic cleavage (not shown) or excision of the Top1cc by tyrosyl-DNA phosphodiesterase 1 (TDP1) (Sparks & Burgers, 2015) followed by gap filling can repair the DNA while eliminating the ribonucleotide.

G When the sequential Top1 cleavage is on the opposite strand to the 2′,3′-CP, a DSB is formed.

H Such Top1-linked DSBs can cause replication stress and lead to recombinations. Adapted from Pommier *et al* (2016).